Nanoscale

Accepted Manuscript

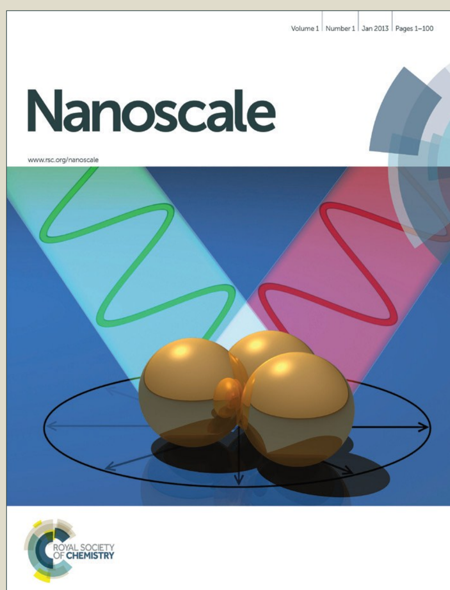

This is an *Accepted Manuscript*, which has been through the Royal Society of Chemistry peer review process and has been accepted for publication.

Accepted Manuscripts are published online shortly after acceptance, before technical editing, formatting and proof reading. Using this free service, authors can make their results available to the community, in citable form, before we publish the edited article. We will replace this *Accepted Manuscript* with the edited and formatted *Advance Article* as soon as it is available.

You can find more information about *Accepted Manuscripts* in the Information for Authors.

Please note that technical editing may introduce minor changes to the text and/or graphics, which may alter content. The journal's standard Terms & Conditions and the Ethical guidelines still apply. In no event shall the Royal Society of Chemistry be held responsible for any errors or omissions in this *Accepted Manuscript* or any consequences arising from the use of any information it contains.

ROYAL SOCIETY OF CHEMISTRY

www.rsc.org/nanoscale

Directly correlating the strain-induced electronic property change to the chirality of individual single-walled and few-walled carbon nanotubes

Zhiyuan Ning[1,#], Qing Chen[1,#,*], Jiake Wei[2], Rufan Zhang[3], Linhui Ye[1], Xianlong Wei[1], Mengqi Fu[1], Yao Guo[1], Xuedong Bai[2, 4] and Fei Wei[3]

[1]Key Laboratory for the Physics and Chemistry of Nanodevices, Department of Electronics, Peking University, Beijing 100871, P. R. China

[2]Institute of Physics, Chinese Academy of Sciences, Beijing 100190, China

[3]Beijing Key laboratory of Green Chemical Reaction Engineering and Technology, Department of Chemical Engineering, Tsinghua University, Beijing 100084, China

[4]Collaborative Innovation Center of Quantum Matter, Beijing, China

[#]The two authors contributed equally.

Abstract: We fabricate carbon nanotube (CNT)-field effect transistors (FETs) with a changeable channel length and investigate the electron transport properties of single-walled, double-walled and triple-walled CNTs under uniaxial strain. Specially, we characterize the atomic structure of the same CNTs in the devices by transmission electron microscopy and correlate the strain-induced electronic property change to the chirality of the CNTs. Both the off-state resistance and on-state resistance are observed to change with the axial strain following an exponential function. The strain-

Nanoscale Accepted Manuscript

induced band gap change obtained from the maximum resistance change in the transfer curve of the ambipolar FETs is quantitatively compared with the previous theoretical prediction and our DFTB calculation from the chirality of the CNTs. Although following the same trend, the experimental obtained strain-induced band gap change is obviously larger (57%-170% larger) than the theoretical results for all the six CNTs, indicating more work is needed to fully understand the strain-induced electronic property change of CNTs.

Keywords: electrical properties, CNT, strain, chirality, *in situ* SEM, nanodevices

Due to their ultra small mass and excellent mechanical, electronic and electromechanical properties, carbon nanotubes (CNTs), and in particular single-walled carbon nanotubes (SWCNTs), are ideal materials for highly efficient sensing devices. Force sensors,[1-3] displacement sensors,[3-5] pressure sensors[6, 7] and strain sensors [8-10] with extra high sensitivity have been demonstrated based on CNTs in the last ten years. For these applications, strain-sensitive electronic property of the CNTs is the most important property. Based on tight-bonding (TB) model, density-functional theory (DFT) or GW approximation (GWA), theoretical works predict that the strain-induced band gap change[11-15] and effective mass change[16] depends strongly on the structure of SWCNTs. When a strain is applied to a SWCNT, its band gap can increase, decrease or remain constant depending on the chirality of the CNT. Many experimental works have observed the conductance change with strain in CNTs by two-terminal electrical measurement.[4-9, 17-20] A couple of three-terminal electrical measurement results qualitatively agree with the theoretical predictions on the strain-induced band gap change ($dE_g/d\varepsilon$).[10, 21, 22] However, almost all these experimental

Nanoscale Accepted Manuscript

works cannot provide the chirality of the CNTs (although the diameter of the CNTs has been measured), so that cannot compare their results with theoretical predictions in a real quantitative way. Through Rayleigh scattering spectroscopy study, the chirality of the CNTs have been measured together with the strain-induced shifts, but the results suggested that the theoretical treatments significantly overestimate the strain-induced energy shifts.[23] Through *in situ* three-terminal electrical measurement using nanoprobes inside a scanning electron microscope (SEM), we have measured the electronic property change with the axis strain of a (20, 13) SWCNT and measured its chiral angle by transmission electron microscopy (TEM).[24] In contrast to the results provided by Ref. 23, our results suggested that the theoretical prediction underestimates the strain-induced band gap change.[24] Recently, the strain-induced band gap change for one specific SWCNT (24, 20) has also been measured using a MEMS structure and compared with the calculation results from the chirality measured by TEM, the experimental value was obviously larger than the theoretically predicted value,[25] which agrees with our previous results. Here, using our newly developed *in situ* platform inside a SEM,[26] we fabricate CNT field effect transistors (FETs) with a changeable channel length, systematically study the transport property of individual suspended CNTs in the FETs at different axial strains and correlate them with the chirality of the CNTs characterized by TEM. We also calculate the $dE_g/d\varepsilon$ of three CNTs we measured using DFTB method (http://www.dftb-plus.info/). Quantitative comparing our experimental results with the existing theoretical predictions and our calculation indicates that $dE_g/d\varepsilon$ has been obviously underestimated by the theoretical works and more work is needed to fully understand the strain-induced electronic property change of CNTs.

Nanoscale Accepted Manuscript

To fabricate a FET with a changeable channel length, a three-terminal structure with a trench located between the metal source (S) and drain (D) electrodes, a narrow slit in the trench, and a highly doped Si gate beneath a 500 nm thick SiO_2 layer was installed on our newly developed platform inside a SEM (FEI Quanta 600 FEG), as shown in Figure 1(a).[3, 26] A side view of the actual experimental setup is shown in Figure 1(b). Individual CNTs were then placed across the S and D electrodes by nanomanipulation to construct a FET device.[3, 24, 26] Figures 1(c) and 1(d) show a schematic diagram (c) and a SEM image (d) of the FET with a suspended CNT. The depth of the trench under the CNT is about 200-300 nm. Driven by the piezoelectric ceramic (PC) in the platform as shown in Figure 1(a), the CNT is stretched precisely by changing the distance between the S and D electrodes[3, 26] and its electrical property is measured at each strain. The suspended length is measured by SEM observation. Importantly, by transferring the neighboring segments on both sides of the same individual CNT used in the devices onto a holey carbon film on a TEM grid,[24] we obtain the atomic level structure (including the diameter and the chirality) of the CNTs in the devices. In such a way, we correlate the strain-induced electronic property change to the chirality of the CNTs, and quantitatively compare the experimental results with the theoretical prediction.

We totally study six suspended CNT-FETs, including two SWCNT-FETs (named as S1 and S2), three DWCNT-FETs (named as, D1, D2 and D3) and one triple-walled CNT (TWCNT)-FET (named as T), respectively. The CNTs in these devices are named as SWCNT1, SWCNT2, DWCNT1, DWCNT2, DWCNT3 and TWCNT, respectively. The diameter and chirality of these CNTs are determined from their high resolution TEM images and electron diffraction patterns as shown in the insets of Figure 2.[27] The detailed process to determine the chirality is given in Supporting

Nanoscale Accepted Manuscript

Information I. The structure parameters of the CNTs together with their suspended length in the devices are listed in lines 1 to 4 in Table 1.

Driven by the PC in the platform, the CNTs are strained along its axis direction. The I_d-V_d curves of the devices measured at V_g=0 V (shown in Figure 2(a)-(f)) and the current at a fixed bias voltage (Supporting Information II, Figure S1) are observed to change reversibly with the strain during repeatedly stretching and releasing the CNTs in the devices. The details on strain measurement are given in Supporting Information III. The reversible results indicate the electrical and physical contacts between the CNTs and the metal electrodes are stable, supporting the reliability of the present results. When the tensile strain increases, the current at a fixed V_d decreases and the resistance increases for all the other five CNTs except that the resistance of SWCNT2 decreases. Such changing trends agree with the theoretical prediction based on the structure of the CNTs.[11] The I_d-V_d curves are nonlinear due to the existence of a contact barrier at the S and D contacts. The contact barrier comes from two main reasons. First, the I_d-V_d curves were measured at V_g=0 V, in which case the devices are at near off-state (as shown later), so that there is a potential barrier at the contact. Second, the CNTs were placed on top of the pre-fabricated S and D electrodes in the present FETs, so that there could be a thin interface layer between the CNT and the Pd electrodes.

The transfer curves at V_d= 0.1 V measured from the six devices without strain are shown as the red thick lines in Figure 3 (a)-(f). The current in device D3 cannot be modulated by the gate voltage, agreed with the fact that the outer layer of DWCNT3 is a small-gap semiconducting (SGS) (15, 12) nanotube. All the other devices have obvious on and off states, agreed with the structure characterization results showing that all these CNTs have semiconducting outer tube.[28, 29] Ambipolar character is

Nanoscale Accepted Manuscript

observed in all these devices, indicating either electron or hole conducts at large positive or negative gate voltage, respectively. The lowest current, so that the maximum resistance, happens at around V_g=0.5 V. Therefore, the I_d-V_d current shown in Figure 2 are in fact measured at near off-state with hole conducting.

When an axis strain is applied, both the on-state current and off-state current change with the strain in all the six devices. When the strain increases, the current in all the devices (including D3) decreases except that the current of device S2 increases, agreed with the theoretical prediction based on the chirality of the CNTs.[11] The current in the SGS CNT in D3 cannot be modulated by V_g when the strain increases from 0 to 1.8% due to the small band gap. Ambipolar character is also observed in D3 when the strain is larger than 2.1% due to the strain-induced band gap increase.

The maximum resistances at each axis strain are obtained from Figure 3 and are plotted in Figure 4 as the square dots. Similar to the previous works,[21, 22] the maximum resistance changes with the axis strain can be fitted well by the following function:

$$R_{max} = R_0 + R_1 \exp(\beta\varepsilon) \qquad (1)$$

From the fitting (the red lines in Figure 4), R_0, R_1 and β are obtained and listed in lines 6 to 8 in Table 1.

We also observe that not only the maximum resistance in the off-state, but the resistance in the on-state also changes with the applied strain, as shown in Figure 3. Strain-induced on-state current change can be noticed in reference 21, but there is no analysis given there. However, the on-state current in reference 22 remains unchanged with the strain. We observe that the on-state resistance changes with the strain in a similar way as the off-state resistance, following the function:

Nanoscale Accepted Manuscript

$$R_{on} = R_{on0} + R_{on1} \exp(\beta^{'} \varepsilon) \qquad (2)$$

where $R_{\text{on}0}$ is a series resistance and $R_{\text{on}1}$ is a parameter not changing with the strain. Fitting the experimental data of Device S1, S2, D1 and T using Eq. (2) (the green and the blue lines in Figure 4 for the n-type and the p-type on-states, respectively), $R_{\text{on}0}$, $R_{\text{on}1}$ and $\beta^{'}$ are obtained for both the n-type and the p-type on-states and are listed in Table 1 in lines 9 to 14. Similar to the off-state, these data are different for different CNTs. For the SGS CNT D3, there is not a current change with the gate voltage at small strain, so that the fitting data for the on-state is the same as that for the off-sate. The on-state resistance of D2 changes roughly linearly with the strain in the on-state, resulting in a large error for fitting with an exponential function, so that we do not list them in Table 1.

Thus, we provide sets of well-controlled experimental data. This is the first time that the experimentally measured strain-induced electronic property changes of several CNTs (including SWCNT, DWCNT and TWCNT) are correlated with the experimentally measured chirality of the CNTs. The present CNTs also include several types: semiconducting with n-m=3q+1, semiconducting with n-m=3q-1 and SGS. And the outer layer of DWCNT1 is the same as SWCNT1. These data allow us to quantitatively compare the experimental results with the theoretical predictions.

Considering that the devices have an almost symmetric ambipolar character, the Fermi level of the S/D electrodes should locate near the middle of the CNT band gap, we can draw the energy band diagrams for the present devices like that shown in Figure 5. That the Pd electrodes (which have a high work function) do not form p-type devices with the CNTs presently is probably because there is an interface layer between the Pd electrode and the CNT. Through fabricating and measuring normal FETs on a substrate, we confirm that when the CNT does not contact directly with

Nanoscale Accepted Manuscript

clean Pd, ambipolar character is obtained. The total resistance of the present devices (R_t) is therefore the sum of the resistance of the CNT channel (R_{ch}), the series resistance in the circuit (R_{cir}), the resistance of the thin interface layer at the contact (R_{in}) and the resistance due to the potential barrier between the Fermi level of Pd and the band edge of the CNT (R_b), as expressed below:

$$R_t = R_{ch} + R_{in} + R_b + R_{cir} \quad (3)$$

Considering the repeatable current response to the strain (Supporting Information II, Figure S1), R_{in} and R_{cir} can be treated being unchanged with the strain. Therefore, the strain-induced resistance change is caused by the change of R_b and R_{ch} with the strain in both the on-state and the off-state.

In the off-state, it can be assumed that the main resistance comes from the energy barrier at the contacts R_b as shown in Figure 5b, and the strain-induced resistance change inside the CNT channel R_{ch} can be neglected. Therefore, the maximum resistance in the off-state can be expressed as:

$$R_{\max} = R_s + A\exp(\frac{E_g}{2k_BT}) \qquad (4)$$

where A is a parameter not changing with the band gap, T is temperature, k_B is the Boltzman parameter and R_s also does not change with the band gap and is the sum of R_{cir}, R_{in} and R_{ch}. Assuming the band gap changes linearly at small strain, $E_g = E_g^0 + \frac{dE_g}{d\varepsilon}\varepsilon$, where E_g^0 is the band gap at ε=0. We then obtain

$$R_{\max} = R_s + A\exp(\frac{E_g^0}{2k_BT}) * \exp(\frac{1}{2k_BT}\frac{dE_g}{d\varepsilon}\varepsilon) \qquad (5)$$

Comparing with Eq. (1), we can obtain:

$$R_0 = R_s \qquad (6)$$

Nanoscale Accepted Manuscript

$$R_1 = A\exp(\frac{E_g^0}{2k_BT}) \qquad (7)$$

and $$\beta = \frac{1}{2k_BT}\frac{dE_g}{d\varepsilon} \qquad (8).$$

Therefore, from the experimental $R_{\max}$–ε plots, $dE_{gap}/d\varepsilon$ of the six CNTs are obtained and the results are listed line 15 in Table 1.

In the present devices, the CNTs are suspended, the gate efficiency is relatively low due to the vacuum layer below the CNT and the gate field could be partially screened by the S/D electrodes below the CNT. So that, in the on-state, there is still a relatively thick energy barrier at the contact region, as shown in Figures 5(a) and 5(c). Therefore, although the present CNT is more than 1 μm long and the transport is diffusive, the main resistance in the on-state is still caused by the energy barrier at the contact R_b, and the interface layer R_{in}, resulting in the low on-state current and the low current on/off ratio in the present devices. As R_{in} does not likely to introduce a repeatable strain-induced change, the main source of the strain-induced on-state resistance change should come from the change of R_b. That explains that the strain-induced resistance change factor β in the on-state is roughly the same as that in the off-state for the two SWCNTs. The reason that β for DWCNT and TWCNT in the on-state is smaller than in the off-state will be discussed later.

Although there have been many theoretical work predicting the strain-induced band gap change, most of them are for specific CNTs, such as zigzag CNTs. The available theoretical work that quantitatively predicts the strain-induced band gap change of chiral CNTs is limited. The strain-induced band gap change of semiconducting SWCNT under axial strain has been predicted theoretically based on TB to be:[11, 14]

Nanoscale Accepted Manuscript

$$dE_{gap}/d\varepsilon = \mathrm{sgn}(2p+1)3t_0(1+\nu)\cos(3\theta) \qquad (9)$$

where t_0=2.66 eV is the tight-binding overlap integral, ν=0.2 is the Poisson ratio, θ is the chiral angle, p= -1, 0, 1 determined by n_1-n_2=3q+p, where q is an integer. While the band gap change of SGS CNT with the axis strain has been deduced from the strain-related band gap given theoretically considering symmetry-breaking effects:[12]

$$dE_{gap}/d\varepsilon = \frac{ab\sqrt{3}}{2}\cos(3\theta) \qquad (10)$$

where $a \approx 2.49\,\mathrm{\mathring{A}}$ is the length of the honeycomb unit vector, $b \approx 3.5\,e\mathrm{V}/\mathrm{\mathring{A}}$ is the linear change in the transfer integral with a change in the bond length, θ is the chiral angle. Knowing the chirality of the CNTs from TEM study, and assuming that only the outer layer of the CNTs was strained when we stretched the CNTs, we calculate $dE_{\mathrm{gap}}/d\varepsilon$ of the CNTs using Eq. (9) and (10), and the results are listed in line 16 in Table 1. Note that the $dE_{\mathrm{gap}}/d\varepsilon$ obtained from the experimental results are obviously larger (57%-170% larger, as listed in Table 1, line 18) than the theoretical prediction, although they follow the same trend. Although there are some uncertainties in the present experimental data, which mainly come from the measurement error of the CNT length, they only result in a 4.9-7.5% uncertainty of the $dE_{gap}/d\varepsilon$ of the six CNTs (as listed in Table 1. The details to assess the uncertainty of the experimental results are given in Supporting Information IV). Therefore, the large difference between the experimental results and the theoretical prediction is not due to the uncertainty in the experimental data. Interaction with the surface of the substrate has been proposed to induce anomalously large responses to the strain.[22] However, the present CNTs are suspended, so that their interaction with the substrate surface can be excluded.

Nanoscale Accepted Manuscript

Although the TB models give correct changing trend,[11] which has been confirmed by many works including the present results, they are not meant to be quantitatively accurate to all the CNTs. Theoretically, the transport band gap is equal to the quasiparticle band gap excluding the electron-hole interaction. Therefore, it would be ideal to calculate the band gap by methods such as the GWA.[30] Unfortunately, the unit cell of the CNTs under this study is too big, and typically include thousands of atoms which renders the direct application of the GWA impossible. A good alternative is then the DFT.[31, 32] Although for the absolute value of the band gap, DFT is intrinsically inferior because of the rigorous lacking of the derivative discontinuity in popular functionals such as the local density approximation and general gradient approximations, the strain coefficient, i.e. the ratio of the band gap variation over the value of the external strain, is surprisingly accurate by DFT. In fact, the accuracy of the DFT strain coefficient is comparable to that of the much more sophisticated GWA.[33, 34] Through DFT calculation and includes structural relaxation effect, P. K. Valavala et al. have reported the band gap changes with strain for (n, 0) SWCNTs are about 10% larger than the TB results.[14] Of course, even by DFT the treatment of thousands of atoms is still impractical with fully converged basis set. As a further simplification, we thus use the DFTB method (http://www.dftb-plus.info/) in all our band structure calculations after full structural relaxation.

The merit of the DFTB method is that it combines density functional theory with parametrized tight-binding method, which makes it very efficient for treating huge systems. Nevertheless, since the high efficiency is partially achieved by adapting minimal basis, noticeable errors are unavoidable in the calculated strain coefficients. For small zigzag CNTs, we have compared the DFTB band gaps with those obtained by fully first principles method with converged basis set, and found that the typical

Nanoscale Accepted Manuscript

error is about several tens percent. This error should be smaller for the CNT's in the present study, since with increased CNT radius the TB approximation is expected to be more accurate. At the limit of infinite radius, a SWCNT would become a single graphene layer, for which the TB approximation is known to work very well. Limited by the unit cell of the CNTs, we only calculate the strain-induced bandgap change for SWCNT1 and the outer layer of DWCNT2 and DWCNT3. The results are listed in line 17 in Table 1 and the details are given in Supporting Information V, Figures S2-S4.

Quantitatively, our DFTB calculation give similar results as the TB prediction, but they are both obviously smaller than the present experimental obtained $dE_{\text{gap}}/d\varepsilon$ values for all the six CNTs. Recent many-body *ab initio* calculations on semiconducting zigzag CNTs showed that the dependence of the electronic band gap on strain is more complex than that predicted previously based on TB models or DFT, the fundamental band gap decrease with strain of (17, 0) CNT is about -125 meV/% by DFT calculation, but is -213 meV/% using the many-body GWA.[15] More theoretical work is needed to understand the strain-induced band gap change of chiral CNTs.

From the experimental point of view, there are several other factors could be considered besides the band gap change, such as the possible torsion along the CNT, collapse at the contacts with the electrodes when the CNT is axially stretched,[4, 11, 24] and some other effects as discussed below.

The contact between the CNT and the S/D electrodes, especially at the edge of the metal next to the channel, is very important to the conductance of the CNT device. If the contact is loose and not stable, there could be a sharp change in the strain at the contact before the tensile strain becomes uniform in the suspended CNT part, and the

Nanoscale Accepted Manuscript

current in the CNT could change sharply near the point with zero strain. However, in the present work, we do not observe any sharp change of the current. As shown in Figure S1, the S-D current changes smoothly even at the beginning the tensile strain is applied. The data shown in Figures 2-4 also show a smooth change near the point with zero strain. The repeatable and reversible results we obtained indicate the contacts in the present work are stable and the strain we measured is the strain in the suspended CNT. The way we fabricate the devices and the pre-tension in the CNT in the as-prepared devices (as explained in Supporting Information III) may be helpful for the stable contact.

In the above analysis, we ignore the influence of the inner layer in the DWCNTs and TWCNT. In the present case, the electrodes only contact the outside layer of the CNTs. As there is a structural superlubricity between the incommensurate CNT layers,[35-38] only the outside layer is strained and the electronic property of the inner layers remain constant during *in situ* pulling and releasing experiments. Therefore, although the inner layers contribute the total current,[28, 29] the strain-induced current change in the off-state mainly comes from the strained outside layer. That explains that the strain-induced current change of SWCNT1 is larger than that of DWCNT1 in the off-state, although the outer layer of DWCNT1 is the same as SWCNT1. However, the contribution from the inner layer cannot be ignored in the on-state. We notice that strain-induced resistance change β in the on-state is about the same as that in the off-state in the case of SWCNT, but it is smaller than that in the off-state in the case of DWCNT, and β in the on-state is even less than half of the value in the off-state in the case of TWCNT. These phenomena indicates not only the inner layer contributes to the total current, but the portion of the inner layer contribution also changes with the strain in the on-state.

Nanoscale Accepted Manuscript

Besides the resistance of the potential barrier R_b, the resistance of the CNT in the channel region R_{ch} also changes with the strain. Theoretical study shows that the effective mass changes with the strain.[16] Therefore, the mobility and the conductivity of the CNTs would change with the strain. On the other hand, strain also introduce lattice distortion, which can also be repeatable in the pulling and releasing process. These lattice distortion could cause more scattering so that reduce the carrier mobility and the conductivity. Due to the large contact resistance, the present devices cannot provide much information in these aspects. Further work is undergoing. On the other hand, theoretical work on these aspects is also limited so far.

In conclusion, we correlate the electromechanical property of SWCNTs, DWCNTs and a TWCNT to their atomic structure through an experimental study. The transport properties of the suspended CNTs at different axial strains are measured through FETs with a changeable channel length fabricated and studied on a homemade platform inside a SEM. The transfer curves of these ambipolar FETs show that not only the minimum current in the off-state, but also the on-state current change with the axial strain and follow a similar exponential function. The strain-induced band gap change obtained from the maximum resistance change qualitatively agrees with the theoretical prediction and our DFTB calculation from the chirality of the CNT, but the values are obviously larger (57%-170% larger) than the theoretical predictions for all the six CNTs. Our results indicate more work is needed to fully understand the strain-induced electronic property change of CNTs.

ASSOCIATED CONTENT

Nanoscale Accepted Manuscript

Supporting Information. I. The detailed process to determine the chirality of a CNT. II. Dynamic current response of the suspended CNT to its axial strain. III. The details on strain measurement. IV. The details to assess the uncertainty of the experimental results. V. DFTB calculation results for (19, 12), (13, 12) and (15, 12) SWCNTs.

Acknowledgement

We thank Professors Zhiyong Zhang and Xuelei Liang for useful discussions. We thank Mr. Jiapei Shu for the help for some experimental work. This work was supported by the NSF of China (11374022, 61321001) and the MOST (2012CB932702). Professor Xuedong Bai and Mr. Jiake Wei were supported by the Strategic Priority Research Program of the Chinese Academy of Sciences (Grant No. XDB07030100).

References

1. Sazonova, V.; Yaish, Y.; Ustünel, H.; Roundy, D.; Arias, T. A.; McEuen, P. L. *Nature* **2004**, *431*, 284-287.
2. Moser, J.; Guttinger, J. ; Eichler, A.; Esplandiu, M. J. ; Liu, D. E. ; Dykman, M. I.; Bachtold, A. *Nature Nanotech.*, **2013**, *8*, 493-496.
3. Ning, Z. Y.; Shi, T. W.; Fu, M. Q.; Guo, Y.; Gao, S.; Wei, X. L.; Chen, Q. *Nano Lett.* **2014**, 14, 1221-1227.
4. Stampfer, C.; Jungen, A.; Linderman, R.; Obergfell, D.; Roth, S.; Hierold, C. *Nano lett.* **2006**, *6*, 1449-1453.

Nanoscale Accepted Manuscript

5. Lee, J.-I.; Eun, Y. K.; Choi, J. W.; Kwon, D.-S.; Kim, J. B. *ACS Appl. Mater. Interfaces*, **2014**, 6, 10181-10187.
6. Stampfer, C.; Helbling, T.; Obergfell, D.; Schoberle, B.; Tripp, M. K.; Jungen, A.; Roth, S.; Bright, V. M.; Hierold, C. *Nano lett.* **2006**, *6*, 233-237.
7. Helbling, T.; Roman, C.; Hierold, C. *Nano lett.* **2010**, *10*, 3350-3354.
8. Yamada, T.; Hayamizu, Y.; Yamamoto, Y.; Yomogida, Y.; lzadi-Najafabadi, A.; Futaba, D. N.; Hata, K. *Nat Nanotech.* **2011**, 6, 296-301.
9. Wu, M. H.; Liu, K. H.; Wang, W. L.; Sui, Y.; Bai, X. D.; Wang, E. G. *Nano Res.* **2012**, 5, 443-449.
10. Cao, J. E.; Wang, Q.; Dai, H. J. *Phys. Rev. Lett.* **2003**, 90, 157601.
11. Yang, L.; Han, J. *Phys. Rev. Lett.* **2000**, 85, 154-157.
12. Kleiner, A.; Eggert, S. *Phys. Rev. B* **2001**, 63, 073408.
13. Ding, J. W.; Yan, X. H.; Cao, J. X. *Phys. Rev. B* **2002**, 66, 073401.
14. Valavala, P. K.; Banyai, D.; Seel, M.; Pati, R. *Phys. Rev. B* **2008**, 78, 235430.
15. Spataru, C. D.; Léonard, F. *Phys. Rev. B* **2013**, 88, 045404.
16. Sreekala, S.; Peng, X.-H.; Ajayan, P. M.; Nayak, S. K. *Phys. Rev. B* **2008**, 77, 155434.
17. Tombler, T. W.; Zhou, C. W.; Alexseyev, L.; Kong, J.; Dai, H. J.; Liu, L.; Jayanthi, C. S.; Tang, M. J.; Wu, S. Y. *Nature* **2000**, 405, 769-772.
18. Cullinan, M. A.; Culpepper, M. L. *Phys. Rev. B* **2010**, 82, 115428.
19. Zheng, F.-Z.; Zhou, Z.-Y.; Yang, X.; Tang, Y.-K.; Wu, Y. *Carbon* **2010**, 48, 2169-2174.

Nanoscale Accepted Manuscript

20. Zheng, F. Z.; Zhou, Z. Y.; Senior Member, IEEE; Yang, X.; Tang, Y. K.; Wu, Y. *IEEE T Nanotechnol* **2011**, 10, 694-698.

21. Minot, E. D.; Yaish, Y.; Sazonova, V.; Park, J.-Y.; Brink, M.; McEuen, P. L. *Phys. Rev. Lett.* **2003**, 90, 156401.

22. Grow, R. J.; Wang, Q.; Cao, J. E.; Wang, D. W.; Dai, H. J. *Appl. Phys. Lett.* **2005**, 86, 093104.

23. Huang, M. Y.; Wu, Y.; Chandra, B.; Yan, H. G.; Shan, Y. Y.; Heinz, T. F.; Hone, J. *Phys. Rev. Lett.* **2008**, 100, 136803.

24. Wei, X. L.; Chen, Q.; Peng, L. M.; Cui, R. L.; Li, Y. *Ultramicroscopy* **2010**, *110*, 182-189.

25. Muoth, M.; Chikkadi, K.; Liu, Y., Hierold, C. *Proc. IEEE MEMS* **2013**, 496-499.

26. Ning, Z. Y.; Fu, M. Q.; Shi, T. W.; Guo, Y.; Gao, S.; Wei, X. L.; Chen, Q. *Nanotechnology* **2014**, 25, 275703.

27. Gao, M.; Zuo, J. M.; Twesten, R. D.; Petrov, I.; Nagahara, L. A.; Zhang, R. *Appl. Phys. Lett.* **2003**, *82*, 2703-2705.

28. Wang, S.; Liang, X. L.; Chen, Q.; Zhang, Z. Y.; Peng, L.-M. *J. Phys. Chem. B* **2005**, 109, 17361-17365 (2005).

29. Wang, S.; Liang, X. L.; Chen, Q.; Yao, K.; Peng, L.-M. *Carbon* **2007**, 45, 760-765.

30. Hedin, L. *Phys. Rev.* **1965**, 139, A796-A823.

31. Hohenberg, P.; Kohn, W. *Phys. Rev.* **1964**, 136, B864-B871.

32. Kohn, W.; Sham, L. J. *Phys. Rev.* **1965**, 140, A1133-A1138.

33. Zhu, X. J.; Fahy, S.; Louie, S. G. *Phys. Rev. B* **1989**, 39, 7840-7847.

34. Wei, S.-H.; Zunger, A. *Phys. Rev. B* **1999**, 60, 5404-5411.

Nanoscale Accepted Manuscript

35. Cumings, J.; Zettl, A. *Science* **2000**, 289, 602-604.

36. Huhtala, M.; Krasheninnikov, A. V.; Aittoniemi, J.; Stuart, S. J.; Nordlund, K.; Kaski, K. *Phys. Rev. B* **2004**, 70, 045404.

37. Kis, A.; Zettl, A. *Phil. Trans. R. Soc. A* **2008**, 366, 1591-1611.

38. Zhang, R. F.; Ning, Z. Y.; Zhang, Y. Y.; Zheng, Q. S.; Chen, Q.; Xie, H. H.; Zhang, Q.; Qian, W. Z.; Wei, F. *Nat Nanotech.* **2013**, 8, 912-916.

Nanoscale Accepted Manuscript

Table 1. The channel length and the geometric parameter of the CNTs used in the six devices, the obtained parameter from fitting the experimental data, $dE_{gap}/d\varepsilon$ obtained from fitting the experimental data and the calculated results of $dE_{gap}/d\varepsilon$ using the TB model and DFTB of the six CNTs.

No.		SWCNT1	SWCNT2	DWCNT1	DWCNT2	DWCNT3	TWCNT
1	Channel length(μm)	1.59±0.03	1.64±0.03	1.31±0.03	1.52±0.03	1.50±0.03	1.24±0.03
2	Outer diameter (nm)	2.14	2.47	2.14	1.72	1.86	4.14
3	Inner diameter(nm)	------	------	1.10	1.03	0.96	2.35
4	Chirality	(19,12)	(19,17)	(19,12)/ (9,7)	(13,12)/ (8,7)	(15,12)/ (8,6)	(49,6)/ (33,13)/ (20,14)
5	Band gap of outer layer (eV)	0.34	0.29	0.34	0.42	~0	0.17
6	R_0(kΩ)	992.8	618.0	813.7	787.3	955.4	503.2
7	R_1(kΩ)	265.2	191.5	95.6	543.2	182.7	27.1
8	β	189.8±12.1	-27.8±1.4	126.1±9.5	20.2±1.3	61.5±3.9	289.9±21.8
9	R_{on0}(kΩ) (n)	160.0	173.3	132.9	------	955.4	135.1
10	R_{on1}(kΩ) (n)	28.1	37.5	18.6	------	182.7	8.3
11	β' (n)	179.5±11.5	-26.6±1.4	103.5±7.8	------	61.5±3.9	129.7±9.8
12	R_{on0}(kΩ) (p)	153.5	167.5	122.9	------	955.4	123.9
13	R_{on1}(kΩ) (p)	27.8	33.3	17.3	------	182.7	8.1
14	β' (p)	169.8±10.8	-28.7±1.5	92.2±6.9	------	61.5±3.9	127.7±9.7
15	**Exp. $dE_{gap}/d\varepsilon$ (meV/%)**	**98.2±6.3**	**-14.4±0.7**	**65.2±4.9**	**10.4±0.7**	**31.8±2.0**	**150±11.3**
16	**Theor. $dE_{gap}/d\varepsilon$ predicted by TB (meV/%)**	**36.3**	**-9.2**	**36.3**	**6.6**	**14.4**	**91.5**
17	**Theor. $dE_{gap}/d\varepsilon$ calculated by DFTB (meV/%)**	**35.9**	**------**	**------**	**6.6**	**11**	**------**
18	(Exp-Theor)/Theor (%)	170±17	57±8	80±14	58±11	121±14	64±12

Nanoscale Accepted Manuscript

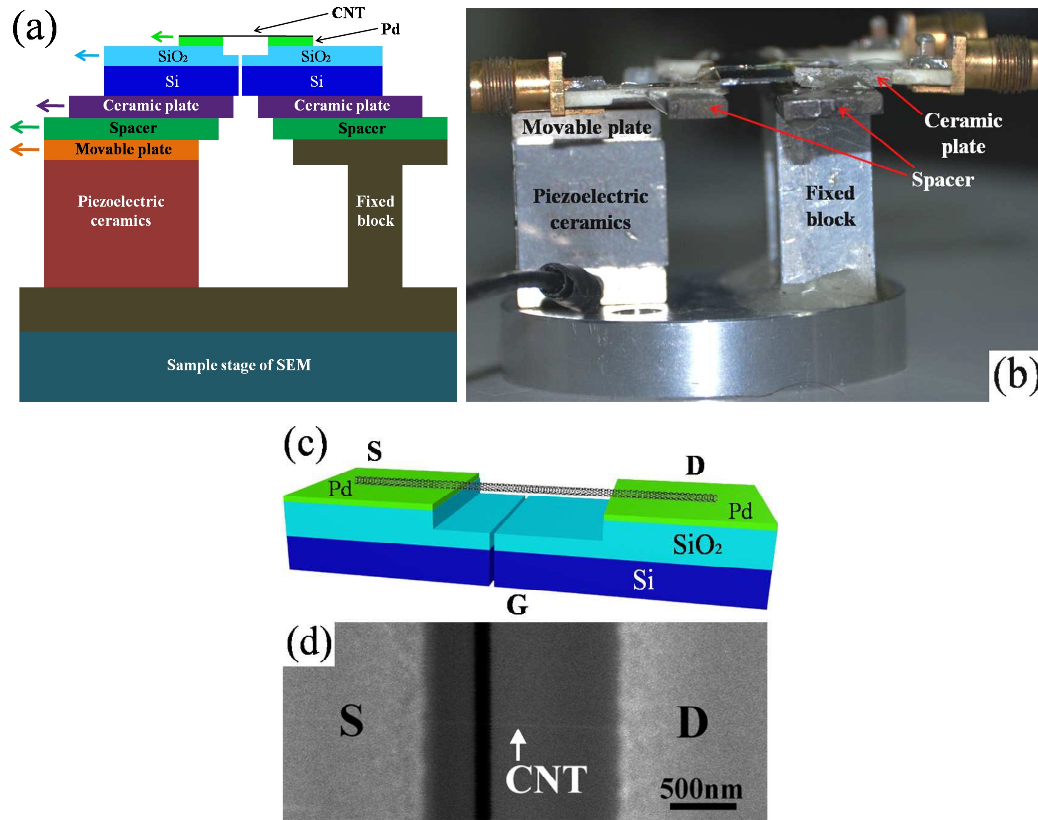

Figure 1. (a) Schematic side view of the three-terminal structure installed on our platform inside the SEM. (b) A photograph of the actual experimental setup. (c) A schematic diagram and (d) a SEM image of a CNT FET device. Due to the same platform used here and in Reference 26, (a) and (b) are similar to Figures 1(a) and 1(f) in Reference 26.

Nanoscale Accepted Manuscript

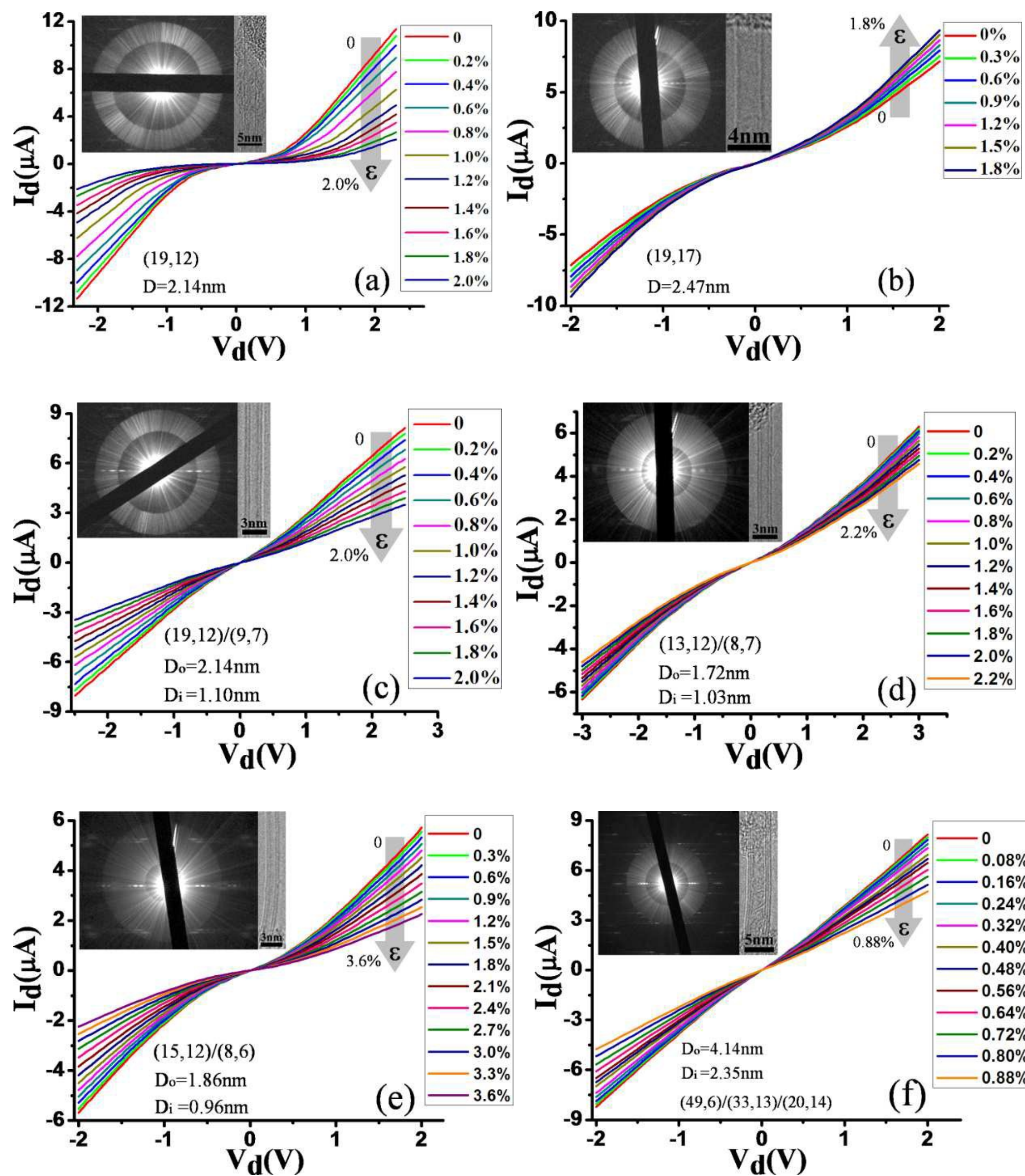

Figure 2. (a)- (f) I_d-V_d curves of Devices S1, S2, D1, D2, D3 and T measured at different strains when V_g= 0 V. The insets are the electron diffraction (left) and high resolution TEM image (right) of the same CNT used in the six devices respectively. The chirality, the outer diameter and inner diameter of the CNTs used in the six devices are also listed in the corresponding I_d-V_d curves. The data in (a) is reproduced from the data shown in Figure 2 in Reference 26.

Nanoscale Accepted Manuscript

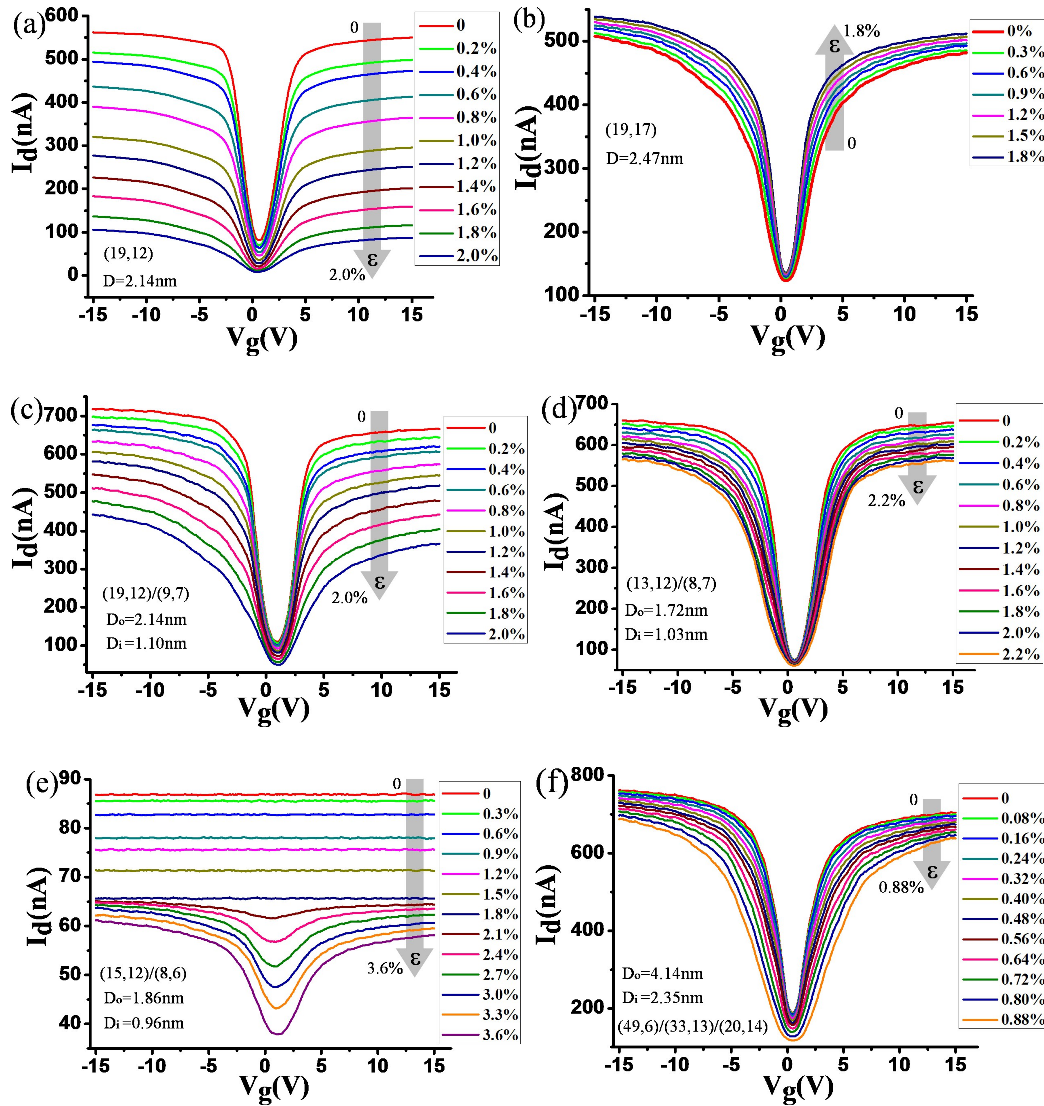

Figure 3. (a)-(f) I_d-V_g curves of Devices S1, S2, D1, D2, D3 and T measured at different strains when V_d= 0.1 V. The chirality, the outer diameter and inner diameter of the CNTs used in the six devices are listed in the corresponding I_d-V_g curves.

Nanoscale Accepted Manuscript

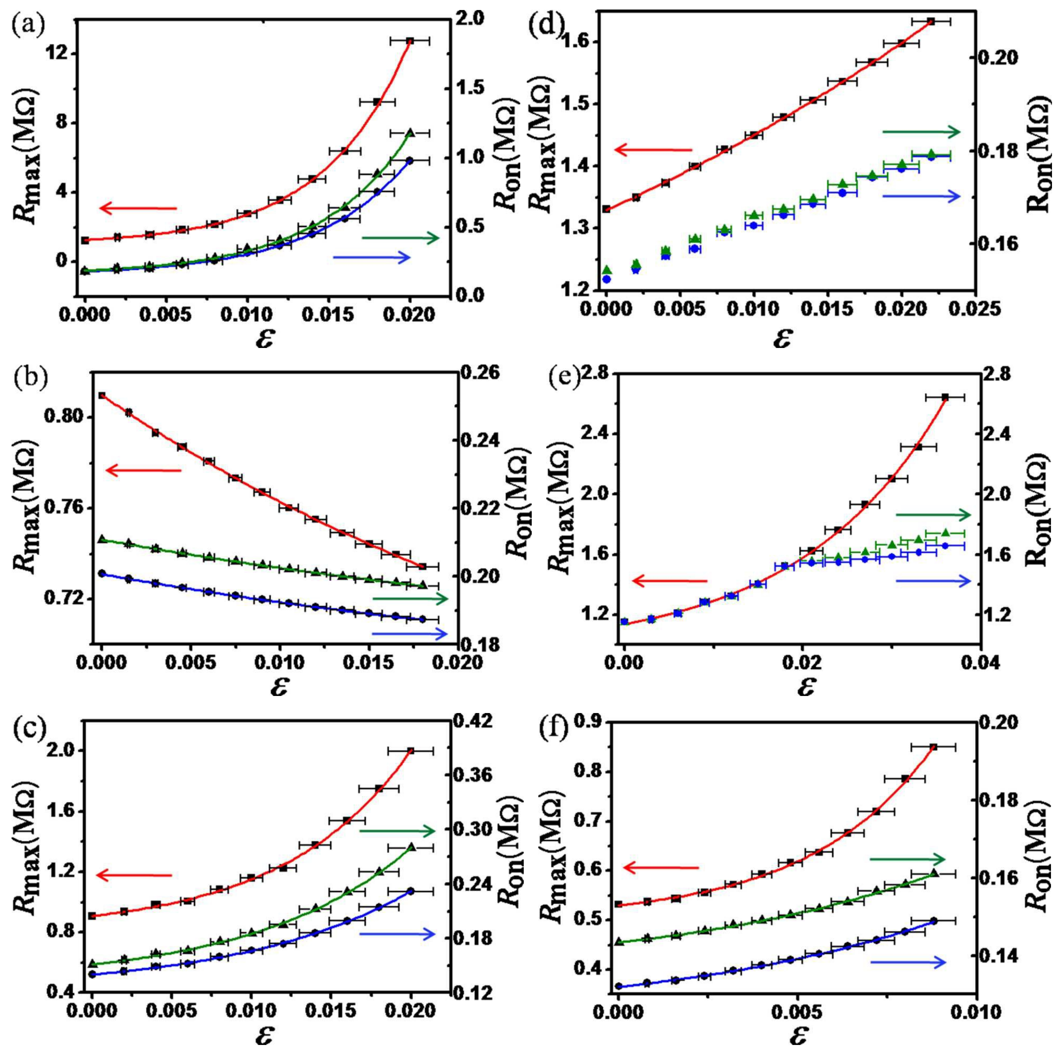

Figure 4. (a) - (f) R_{max}-ε plots and R_{on}-ε plots of Devices S1, S2, D1, D2, D3 and T. The square dots, triangle dots and circular dots are the experimental data of R_{max}, n-type R_{on} and p-type R_{on}. The red solid line is the fitting curve using equation (1). The green and blue solid lines are the fitting curves using equation (2).

Nanoscale Accepted Manuscript

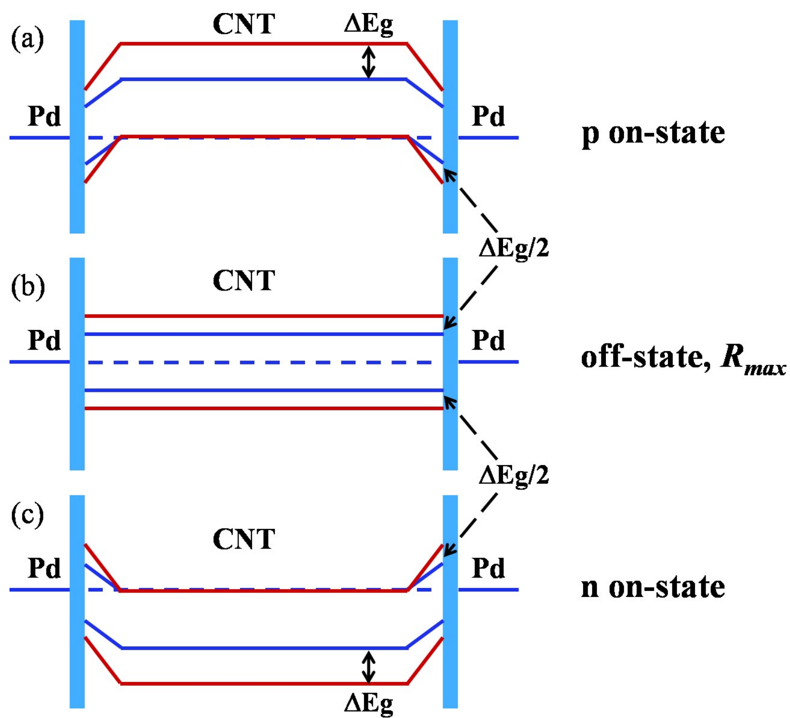

Figure 5. (a), (b) and (c) The energy band diagram of the CNT devices in p-type on-state, off-state and n-type on-state, respectively.

Nanoscale Accepted Manuscript